DESIGN AND DEVELOPMENT OF AN ADHESIVE JOINT TESTING APPARATUS FOR MIXED-MODE EVALUATION

F.J.P. Chaves [1], L.F.M. da Silva [2] ,M.F.M. de Moura [2] and D. Dillard[3]

[1] *IDMEC- Pólo FEUP,Faculdade de Engenharia da Universidade do Porto, Rua Dr. Roberto Frias, 4200-465 Porto, Portugal*
chaves.filipe@fe.up.pt

[2] *DEMec,Faculdade de Engenharia da Universidade do Porto, Rua Dr. Roberto Frias, 4200-465 Porto, Portugal, lucas@fe.up.pt , mfmoura@fe.up.pt*

[3] *Engineering Science and Mechanics Department, Virginia Tech, Blacksburg, VA 24061dillard@vt.edu*

KEYWORDS: Development, Design, Bonded joints, fracture characterization, mixed-mode I+II loading, in-plane mode mixity

ABSTRACT: *The present work is dedicated to the development and design of a load jig inspired in the proposed solution by Fernlund and Spelt in order to characterize fracture of bonded joints under mixed-mode I+II loading. The jig allows for easy alteration of the mode-mixity and permits covering the full range of mixed-mode I+II combinations. A data reduction scheme based on specimen compliance, beam theory and crack equivalent concept is proposed to overcome several difficulties inherent to the test analysis. The development was based in a design methodology using numerical validation based on experimental data obtained with a Dual Loading Frame from Virginia Tech. This methodology is presented and then validated with the experimental application of the jig.*

INTRODUCTION

Bonded joints are being increasingly applied in structures involving risk, as is the case of the aeronautical, automotive, and civil infrastructure industries. The classical strength prediction based on stress or strain analysis may not be adequate in the presence of singularities which occur frequently in bonded joints. As a result, the development of sophisticated design criteria including progressive damage analysis is of fundamental importance. In this context cohesive zone modelling that combine stress-based criteria to simulate damage initiation and fracture mechanics criteria to deal with damage growth acquires special relevancy (Yang and Thouless 2001; Blackman, Hadavinia et al. 2003; Andersson and Stigh 2004; de Moura and Chousal 2006; Campilho, Moura et al. 2008). Fracture mechanics-based criteria require prior characterization of the joint under mixed-mode loading, since bonded joints in real applications often experience such situations.

The objective of this work is to develop a new apparatus for the mixed-mode inspired in the test developed by Fernlund and Spelt (Fernlund and Spelt 1994).

METHODOLOGY

A design methodology based in simulation of the apparatus loading scheme matching the experimental data obtained was implemented and is explained. The loading jig consists primarily of two rigid beams linked to each other, to the specimen, and to a base plate (Figure 1). Different jig geometries can be achieved by altering the four distances, s_1 - s_4, thereby varying the mode-mixity of the

induced loading (Fernlund and Spelt 1994). Changing the above referred distances leads to different loads, F_1 and F_2, applied to the upper and lower adherends, respectively, of the tested specimens (Figure 2). The jig also permits the realization of pure mode tests, namely the Double Cantilever Beam (DCB) for mode I and the End-Notched Flexure (ENF) for mode II, thus being versatile in the context of fracture characterization.

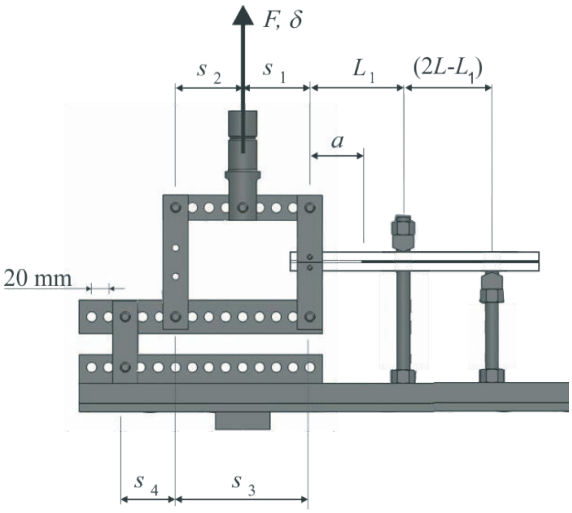

Fig. 1 Load jig.

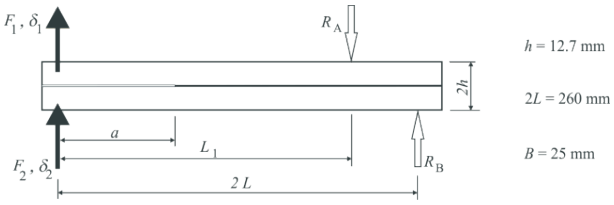

Fig. 2 Schematic representation of specimen loading and dimensions (B is the specimen width).

The different parts were modelled and assembled using Solidworks ® that provided a first simulation approach using springs and connectors to emulate the adhesive. This simulation approach was compared with the results obtained using cohesive elements within ABAQUS ® and the combined results were then compared with the experimental results obtained as shown in Figure 3.

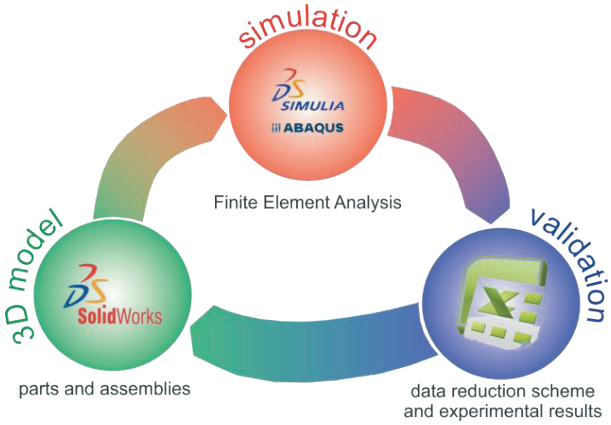

Fig. 3 Design methodology.

ADHESIVE LAYER SIMULATION

Solidworks® and ABAQUS® were used to perform the simulation for the device loading and the specimen adhesive behaviour. The Jig was modelled in Solidworks® because it allows an easier job in designing 3D parts and assemblies. Furthermore this software does not require high level hardware and allows rapid processing times. However, the simulation add-in for Solidworks® does not contemplates cohesive elements, preferred for adhesive behaviour numerical simulations. Instead, spring elements were used to simulate the adhesive behaviour. To determine the spring constant [k] simulations done with ABAQUS® cohesive elements were compared with Solidworks® modelled with springs, for perfect match behaviour as shown in Figure 4.

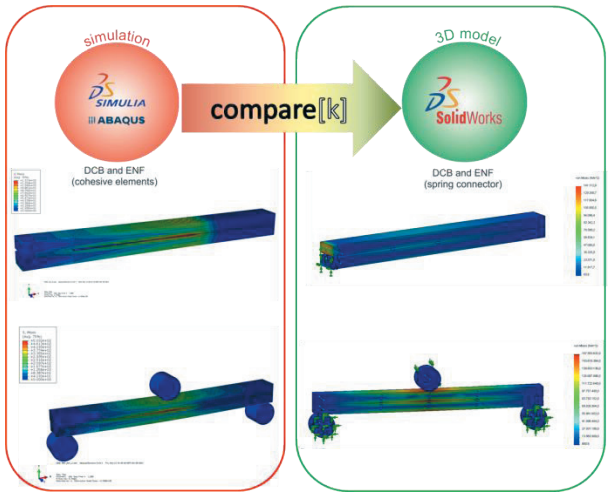

Fig. 4 Comparison between ABAQUS® and Solidworks® models.

3D parabolic tetrahedral elements with 4 Gauss points were used in Solidworks® simulations. The mesh was tuned with the proportion and number of Gauss points and optimized with uniform tetrahedral elements with equal edges. Solidworks® verifies the perfect element proportion in order to guarantee the mesh quality. Table 1 shows the mesh characteristics for Solidworks® simulations.

Table 1. Solidworks® mesh characteristics.

Mesh type	Solid Mesh
Mesher Used:	Curvature based mesh
Jacobian points	4 Points
Max. element size	7.21293 mm
Min. element size	1.44259 mm
Mesh Quality	High

The problem size in Solidworks® is shown in table 2 for DCB and table 3 for ENF specimens.

Table 2. DCB problem size in Solidworks® .

Total Nodes	24264
Total Elements	14980
Maximum Aspect Ratio	4.1124
% of elements with Aspect Ratio < 3	99.4
% of elements with Aspect Ratio > 10	0
% of distorted elements (Jacobian)	0

Table 3. ENF problem size in Solidworks® .

Total Nodes	17909
Total Elements	10478
Maximum Aspect Ratio	4.0217
% of elements with Aspect Ratio < 3	97.7
% of elements with Aspect Ratio > 10	0
% of distorted elements (Jacobian)	0

Adhesive behaviour was simulated with ABAQUS® using C3D8R elements for substrates and COH3D8 for the cohesive elements. C3D8R is a reduced integration linear element appropriated for linear elastic behaviour materials such as steel. To preview the crack propagation a thin mesh with a cohesive element is best suited, thus a COH3D8 cohesive element was used. This cohesive element is governed by a bi-linear traction separation law, as shown in Figure 5 with the damage parameters defined for Araldite® 2015 in Table 4. The problem size in ABAQUS ® is shown in table 5 for DCB and table 6 for ENF specimens. ENF specimen simulation requires more nodes because it defines the contact with the loading rolls.

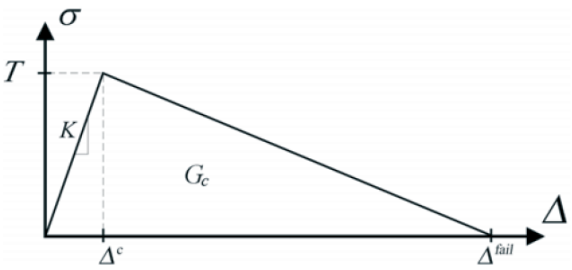

Fig. 5 Bi-linear traction separation law.

Table 4. Cohesive law damage parameters.

Quads Damage	
Nominal Stress Normal-tension	21.64 Mpa
Nominal Stress 1st direction	17.9 MPa
Nominal Stress 2nd direction	17.9 MPa
Damage Evolution	
Normal Fracture Energy	0.43 N/m
Shear Fract. Energy 1st Direction	4.7 N/m
Shear Fract. Energy 2nd Direction	4.7 N/m

Table 5. DCB problem size in ABAQUS® .

Number of nodes	100624
Number of nodes defined by user	100624
Number of elements	87750
Number of elements defined by user	87750
Number of variables in the model	301872

Table 6. ENF problem size in ABAQUS® .

Number of nodes	92199
Number of nodes defined by user	86547
Number of elements	79380
Number of elements defined by user	76551
Internal nodes generated by program	5652
Internal elem. generated for contact	2826
Number of variables in the model	268128

The material for the substrates used in Solidworks® and ABAQUS® is an high grade steel with properties as defined in table 7.

Table 7. Steel properties used for substrates and Jig base.

AISI P20	
Hardness (HB)	290/330
Yield Stress (MPa)	640
Ultimate Fracture Stress (MPa)	993
DIN CK 45	
Hardness (HB)	170
Yield Stress (MPa)	323
Ultimate Fracture Stress (MPa)	578

Results obtained from ABQUS simulations have already been compared and validated with experimental results in a previous work done by da Silva et al.(da Silva, Esteves et al. 2011). Using these results, the spring constant [k] was tuned for DCB and ENF specimens' simulation as seen in Figure 6 with a normal stiffness of 400 N/m, tangential stiffness of 4000 N/m and a tension pre-load force of 300 N.

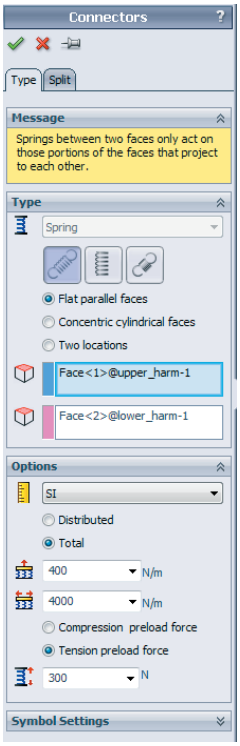

Fig. 6 Spring connector definition in Solidworks®.

NUMERICAL ANALYSIS

DCB and ENF specimens were then used within a Solidworks® assembly of the Jig parts in order to optimize the design of the different mechanical components taking into account the different loading conditions and considering the maximum values for the resulting Von Mises criterion stresses.

Some examples for this approach can be seen in Figures 7 and 8. Figure 7 shows the connector to the Universal Testing Machine with the plot of the results for stresses (left) and displacements (right).

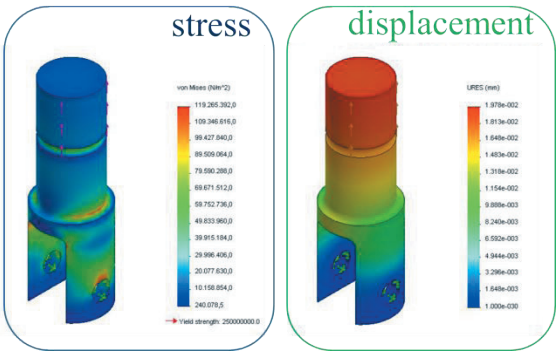

Fig. 7 Stress and displacement plots for the connector to the Universal Testing Machine.

The Jig base which supports the device weight is shown in Figure 8.

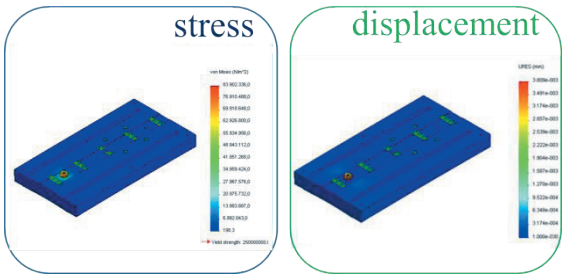

Fig. 8 Stress and displacement plots for Jig base.

By analysing the stress and displacement values obtained, each component was optimized in terms of geometry and material, trying to obtain the less expensive solution without compromising the assembly stiffness, avoiding plasticity. For example, the base was manufactured with a less expensive mild steel (DIN CK 45) to reduce production and material costs, and the connector to the universal machine was geometrically optimized using a high grade and more expensive steel (AISI P20) with properties defined in Table 7. Each part was simulated individually and then within the assembly to validate the overall results using an iterative method as shown in Figure 3.

DATA REDUCTION SCHEME

After the optimization design phase with the Jig geometry fully defined, it was possible to simulate the behaviour using different cohesive laws and to obtain a numerical envelope to compare with the experimental results. A data reduction scheme was also developed to improve the test practicability. The classical data reduction schemes based on compliance calibration and beam theories are based on crack length monitoring during its propagation. However, there are two limitations related to this aspect. In fact, this task is not easy to be accomplished with the required accuracy namely in cases where mode II loading predominate, since the crack faces remain in contact during its propagation. The second limitation is related to the energy dissipation at the fracture process zone (FPZ) ahead of the crack tip, which can be non-negligible as is the case of adhesives with some inelastic behaviour. The consideration of the clear crack length (not including the influence of the FPZ size), as a fracture parameter in beam theory equations does not allow accounting for this energy. An alternative procedure based on an equivalent crack concept can be used with remarkable advantages (de Moura and Chousal 2006). The proposed method is based on Timoshenko beam theory and uses the current specimen compliance to estimate an equivalent crack during the test. This method relies on the loads F_1,F_2 calculated from the loading cell as explained by Fernlund (Fernlund and Spelt 1994) and displacements δ_1,δ_2 obtained from two LVDTs (Linear Variable Differential Transformer) seen in Figure 2 and is explained in Figure 9.

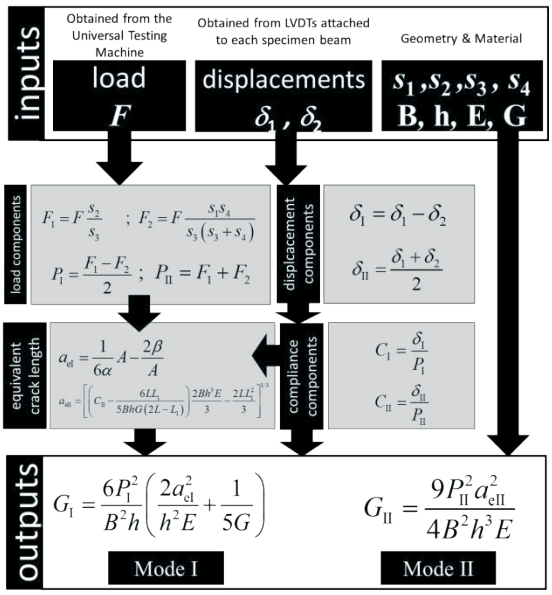

Fig. 9 Data reduction scheme formulation.

To validate the proposed data reduction scheme when applied to this device, seven scenarios were considered in the G_I-G_{II} space, including the pure mode cases. The mode mixity between different scenarios (Table 8) was changed by altering the distances s_1-s_4 (as defined in Figure 1).

Table 8. Different scenarios used for the fracture envelope calculation.

	Jig arrangement			
Scenarios	s_1 **(mm)**	s_2 **(mm)**	s_3 **(mm)**	s_4 **(mm)**
P1	100	40	140	-60
P2	120	40	160	-120
P3	40	120	160	40
P4	60	80	140	60
P5	60	80	140	120
P6	40	40	80	100
P7	100	40	140	80

The classical compliance calibration method (CCM) was also applied to the numerical results to validate the proposed CBBM. This method is easy to apply numerically, since the crack length can be straightforwardly monitored, which does not happen experimentally. Using the Irwin-Kies relation G_T becomes

$$G_T = \frac{F_1^2}{2B}\frac{dC_1}{da} + \frac{F_2^2}{2B}\frac{dC_2}{da} \qquad (1)$$

The different cohesive laws used for the simulations were the linear law as defined in Eq. 2 and the quadratic law defined by Eq. 3.

$$\left(\frac{G_I}{G_{Ic}}\right) + \left(\frac{G_{II}}{G_{IIc}}\right) = 1 \qquad (2)$$

$$\left(\frac{G_I}{G_{Ic}}\right)^2 + \left(\frac{G_{II}}{G_{IIc}}\right)^2 = 1 \qquad (3)$$

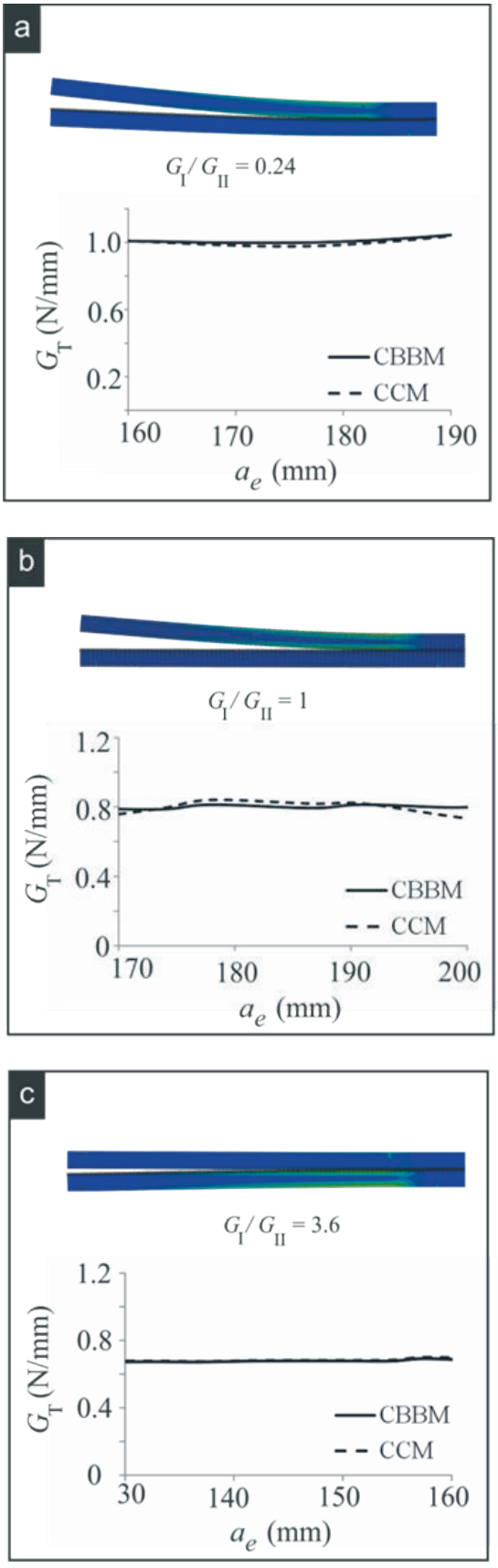

Fig. 10 Plot of the $G_T = f(a_e)$ curves obtained by the CCM and the CBBM for G_I/G_{II}=0.24 (scenario P7) ; G_I/G_{II}=1 (scenario P4) and G_I/G_{II}=3.6 (scenario P1).

The curves $G_T = f(a_e)$ obtained by the CCM and the CBBM are plotted in Figure 10, considering the three representative cases of mode-mix, for the range of a_e corresponding to crack growth. Although the CCM is a function of a, the a_e was used to provide better comparison between the two methods. It can be concluded that both methods provide results that are in close agreement, thus validating the proposed CBBM. The R-curves were also obtained for the remaining mixed-mode combinations. The main goal was to verify whether the linear energetic criterion considered in the numerical simulations is well reproduced when applying the proposed data reduction scheme to the numerical results, i.e., the applied load P and the resultant displacements of each arm, δ_1 and δ_2. With this aim, the values issuing from the plateau of the R-curves are plotted in a graph of the G_I-G_{II} space (Figure 11) and compared to the straight line representing the linear energetic criterion (Eq. 2). A similar procedure was followed using the quadratic energetic criterion (Eq. 3) and considering the same seven scenarios (Table 8). The good agreement obtained for both criteria demonstrates that the proposed model can be applied with success as a straightforward data reduction scheme for the present mixed-mode I+II fracture characterization test.

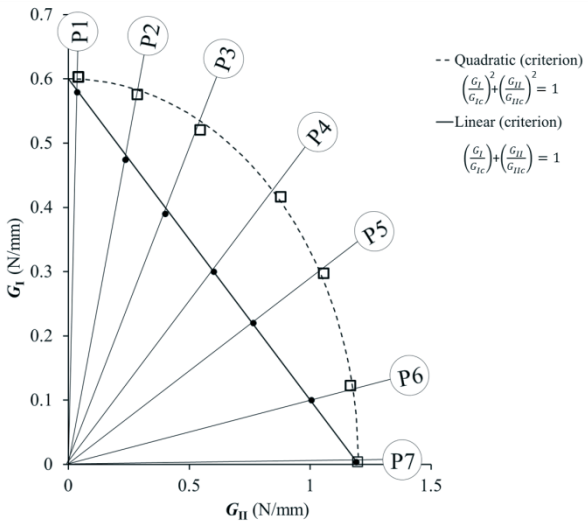

Fig. 11 Fracture envelope for the seven scenarios analysed considering the linear (●) and quadratic (◘) criteria.

An adhesive with different properties, shown in Table 9 was used to compute these simulations.

Table 9. Adhesive properties.

Adhesive Properties	
Normal Fracture Energy	0.6 N/m
Shear Fract. Energy 1st Direction	1.2 N/m
Shear Fract. Energy 2nd Direction	1.2 N/m

EXPERIMENTAL RESULTS

Working with the Jig, already mounted in a Universal Testing Machine, it was possible to conduct several tests to experiment the suitability of this design.

Three combinations for the s_1-s_4 dimensions were tested, to obtain the opening pure mode I were set as s_1=40 mm , s_2 =120 mm, s_3=160 mm and s_4 = -120 mm and The remaining two combinations, were set in order to obtain a predominant mode I test - s_1=60 mm , s_2 =100 mm, s_3=160 mm and s_4 = 80 mm - as a second set-up with ψ = 20º and the third set-up to obtain a predominant mode II test with ψ = 85º - s_1=80 mm , s_2 =60 mm , s_3=140 mm and s_4 = 100 mm. The nominal phase angle of loading ψ, as defined by Fernlund and Spelt (Fernlund and Spelt 1994) is also an important value, helping to discriminate each loading case, and is defined by:

$$\psi = \arctan\left(\sqrt{G_{II}/G_I}\right);\ \psi = \arctan\left[\frac{\sqrt{3}}{2}\frac{\left(\frac{F_1}{F_2}+1\right)}{\left(\frac{F_1}{F_2}-1\right)}\right] \quad (16)$$

The load-displacement (F-δ) curve obtained from the universal testing machine and also the displacements (δ_1 and δ_2) recorded by the LVDTs at the loading pins, for the first apparatus set up (s_1=40 mm , s_2 =120 mm , s_3=160 mm and s_4 = -120 mm) are shown in the graph of Figure 12. Using this data to

calculate the energy release rate, it was possible to compute the R-curve for this loading case as shown in Figure 13. The nominal phase angle of loading ψ for this case is 0º.

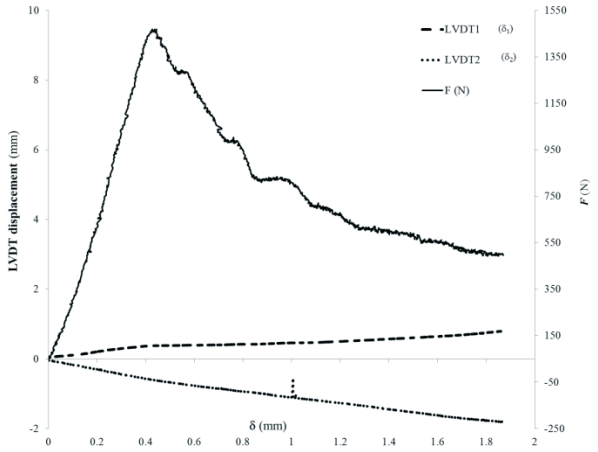

Fig. 12 Load displacement and LVDTs displacement curves for pure mode I loading case (s_1=40 mm , s_2 =120 mm , s_3=160 mm and s_4 = -120 mm), ψ = 0º.

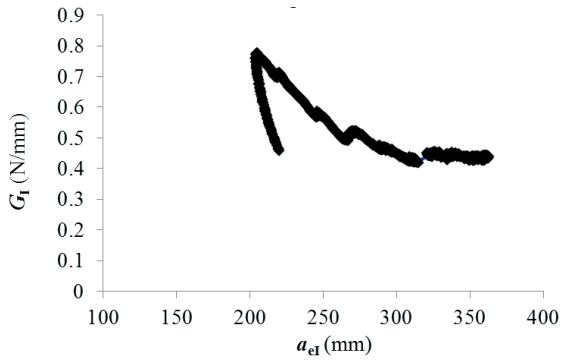

Fig. 13 R-curve for the first loading case (pure mode I, s_1=40 mm , s_2 =120 mm , s_3=160 mm and s_4 = -120 mm).

The computed energy release rate for this test is plotted in Figure 13 and shows a blunt effect caused by the round tip of the initial crack, and then stabilizes at a plateau near 0.438 N/mm for the mode I energy release rate, G_I. This value is in agreement with previously works published by da Silva et al. (da Silva, Esteves et al. 2011) and Campilho , Moura et al. (Campilho, Moura et al. 2008).

The second loading case, (s_1=60 mm, s_2 =100 mm, s_3=160 mm and s_4 = 80 mm) load-displacement (F-δ) and the specimen beams displacements (δ_1 and δ_2) recorded by the LVDTs at the loading pins, are shown in Figure 14. The nominal phase angle of loading ψ for this case is 20º.

The resulting R-curves for mode I and mode II are plotted in Figure 15.

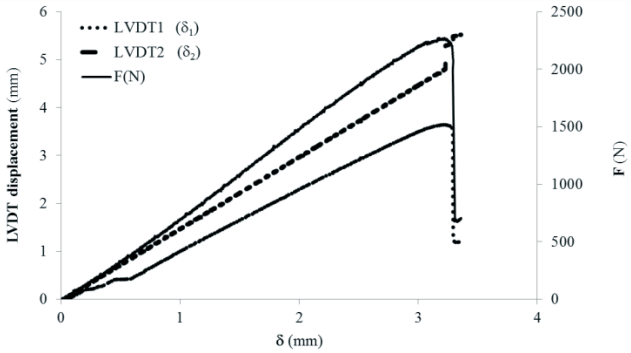

Fig. 14 Load displacement and LVDTs displacement curves for the second loading case (s_1=60 mm , s_2 =100 mm , s_3=160 mm and s_4 = 80 mm), ψ = 20º.

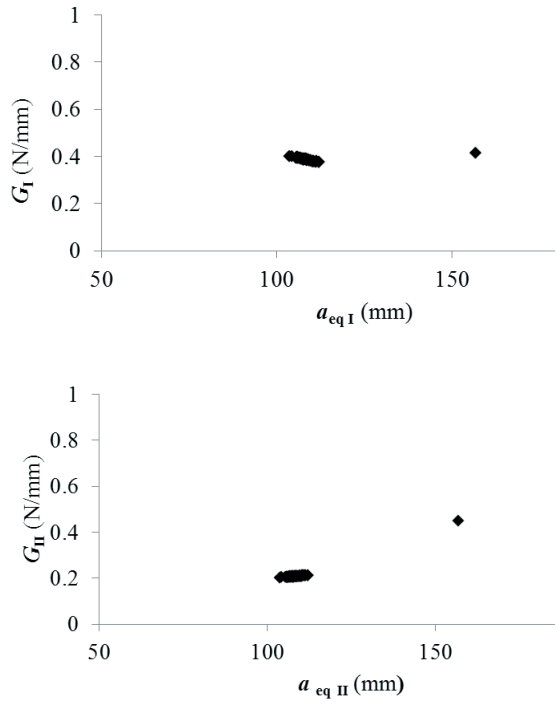

Fig. 15 Mode I (up) and mode II (down) R-curves for the second loading case (s1= 60 mm, s2=100 mm, s3=160 mm and s4 = 80 mm).

Figure 15 (up) shows a plateau near 0.382 N/mm for the mode I energy release rate, G_I and another plateau near 0.22 N/mm for the mode II energy release rate, G_{II} (down). This is in accordance with a mode I predominant test.

For the third loading case (s_1=80 mm, s_2 =60mm , s_3=140 mm and s_4 = 100 mm), the load-displacement (F-δ) and the displacements (δ_1 and δ_2) recorded by the LVDTs at the loading pins, are shown in Figure 16. The nominal phase angle of loading ψ for this case is 85º.

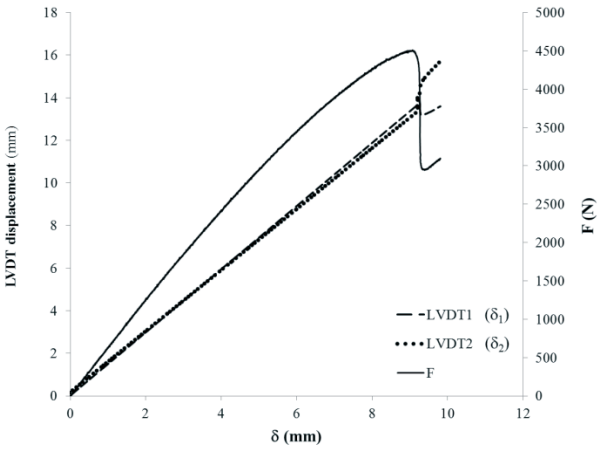

Fig. 16 Load displacement and LVDTs displacement curves for the third loading case (s_1=80 mm, s_2 =60 mm, s_3=140 mm and s_4 = 100 mm), ψ = 85º.

Computing this data with the proposed data reduction scheme, the resulting R-curves for mode I and mode II are plotted as shown in Figure 17.

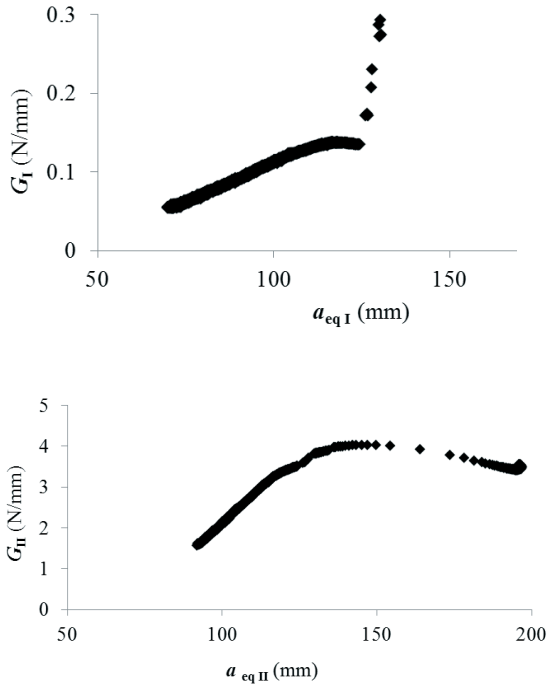

Fig. 17 Mode I (up) and mode II (down) R-curves for the third loading case (s_1=80 mm, s_2 =60 mm, s_3=140 mm and s_4 = 100 mm).

Figure 17 (up) shows a plateau near 0.13 N/mm for the mode I energy release rate, G_I , and another plateau near 3.42 N/mm for the mode II energy release rate, G_{II} (down). The higher value for G_{II} is in accordance with a mode II predominant test as expected.

Using the previous information, it is possible to obtain a fracture envelop with these three points of the energy release rate in mode I (G_I) and mode II (G_{II}) for each combination as shown in Figure 18.

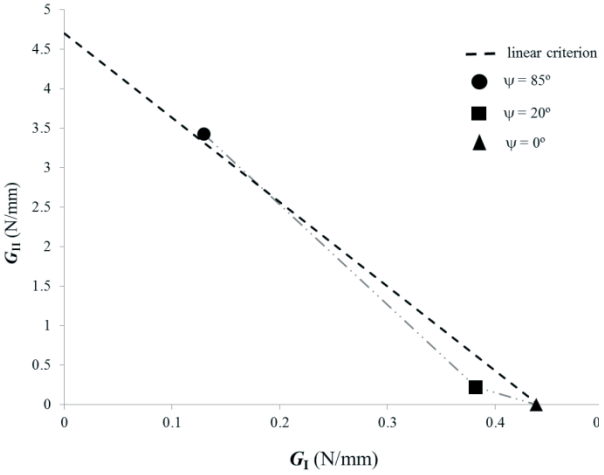

Fig. 18 Fracture envelop for the three combinations (ψ = 85º, ψ = 20 º and ψ = 0º).

This fracture envelope shows a correct relative positioning for each test and a moderate accordance with the linear criterion defined in Eq. 2.

CONCLUSIONS

The development of the testing apparatus for the mixed-mode I + II fracture mechanics evaluation of adhesive joints benefited of a design methodology based in numerical simulation using Finite Element Analysis. This methodology allowed the validation prior to manufacture, avoiding errors and also allowing the optimization of materials and parts geometry.

While at the simulation stage it was also developed a data reduction scheme that improves the efficiency of the test, benefiting of the same design methodology. This data reduction scheme was first validated recurring to numerical results and later used to analyse experimental results with good results.

The Jig was manufactured and used to obtain experimental results confirming its adequacy and novelty for the adhesive joints mixed-mode evaluation allowing to validate the data reduction scheme and obtain a full fracture envelope.

ACKNOWLEDGEMENTS

The authors would like to thank the "Fundação Luso-Americana para o Desenvolvimento" (FLAD) for the support through project 314/06, 2007 and Instituto de Engenharia Mecânica (IDMEC).

REFERENCES

Andersson, T. and U. Stigh (2004). "The stress-elongation relation for an adhesive layer loaded in peel using equilibrium of energetic forces." International Journal of Solids and Structures **41**(2): 413-434.

Blackman, B. R. K., H. Hadavinia, et al. (2003). "The use of a cohesive zone model to study the fracture of fibre composites and adhesively-bonded joints." International Journal of Fracture **119**(1): 25-46.

Campilho, R. D. S. G., M. F. S. F. d. Moura, et al. (2008). "Obtaining the cohesive laws of a trapezoidal mixed-mode damage model using an inverse method." Ciência & Tecnologia dos Materiais **20**: 81-86.

da Silva, L. F. M., V. H. C. Esteves, et al. (2011). "Fracture toughness of a structural adhesive under mixed mode loadings

Bruchzähigkeit eines Strukturklebstoffs bei Mixed-Mode Belastung." Materialwissenschaft und Werkstofftechnik **42**(5): 460-470.

de Moura, M. F. S. F. and J. A. G. Chousal (2006). "Cohesive and continuum damage models applied to fracture characterization of bonded joints." International Journal of Mechanical Sciences **48**(5): 493-503.

Fernlund, G. and J. K. Spelt (1994). "Mixed-mode fracture characterization of adhesive joints." Composites Science and Technology **50**(4): 441-449.

Yang, Q. D. and M. D. Thouless (2001). "Mixed-mode fracture analyses of plastically-deforming adhesive joints." International Journal of Fracture **110**(2): 175-187.